Environmental Toxicology and Pharmacology 47 (2016) 108–118

Contents lists available at ScienceDirect

Environmental Toxicology and Pharmacology

journal homepage: www.elsevier.com/locate/etap

Influence of silver and titanium dioxide nanoparticles on *in vitro* blood-brain barrier permeability

I-Chieh Chen, I-Lun Hsiao, Ho-Chen Lin, Chien-Hou Wu, Chun-Yu Chuang*, Yuh-Jeen Huang*

Department of Biomedical Engineering and Environmental Sciences, National Tsing Hua University, 101, Section 2, Kuang-Fu Road, Hsinchu, 30013, Taiwan

ARTICLE INFO

Article history:
Received 29 April 2016
Received in revised form 31 August 2016
Accepted 14 September 2016
Available online 15 September 2016

Keywords:
Silver nanoparticles
Titanium dioxide nanoparticles
In vitro blood-brain barrier
Permeability
Silver ions

ABSTRACT

An *in vitro* blood-brain barrier (BBB) model being composed of co-culture with endothelial (bEnd.3) and astrocyte-like (ALT) cells was established to evaluate the toxicity and permeability of Ag nanoparticles (AgNPs; 8 nm) and TiO_2 nanoparticles (TiO_2NPs; 6 nm and 35 nm) in normal and inflammatory central nervous system. Lipopolysaccharide (LPS) was pre-treated to simulate the inflammatory responses. Both AgNPs and Ag ions can decrease transendothelial electrical resistance (TEER) value, and cause discontinuous tight junction proteins (claudin-5 and zonula occludens-1) of BBB. However, only the Ag ions induced inflammatory cytokines to release, and had less cell-to-cell permeability than AgNPs, which indicated that the toxicity of AgNPs was distinct from Ag ions. LPS itself disrupted BBB, while co-treatment with AgNPs and LPS dramatically enhanced the disruption and permeability coefficient. On the other hand, TiO_2NPs exposure increased BBB penetration by size, and disrupted tight junction proteins without size dependence, and many of TiO_2NPs accumulated in the endothelial cells were observed. This study provided the new insight of toxic potency of AgNPs and TiO_2NPs in BBB.

1. Introduction

Silver and titanium dioxide nanoparticles (AgNPs and TiO_2NPs) are the two most commonly engineered nanoparticles (NPs). AgNPs are regarded as great antibacterial agents, and are used extensively in textiles, masks, medicines, food packages or other spray products (Rai et al., 2009). TiO_2NPs have excellent photocatalytic activity and surface super-hydrophobic capacity so that can apply in paints, ceramic tiles, cosmetics, even food additives (Gupta and Tripathi, 2011). Along with the widely application in nanomaterials, there is numerous researchers have emphasized that these engineered NPs are involved in potential adverse impacts to the environment, health and safety (Maynard, 2014; Song et al., 2009).

In vivo studies have demonstrated that AgNPs and TiO_2NPs can translocate into central nervous system (CNS), and are detected in brain by main routes of introducing NPs into the body *e.g.*, oral (Ag (Loeschner et al., 2011; Park et al., 2010); TiO_2 (Ze et al., 2014b)), inhalation administration (Ag (Takenaka et al., 2001)), intranasally instillation (Ag (Genter et al., 2012)), subcutaneous (Ag (Tang et al., 2009)), intragastric (TiO_2 (Hu et al., 2010)) administration. Moreover, AgNPs and TiO_2NPs have been detected in various brain regions such as cerebral cortex, hippocampus, and cerebellum, and can stay in a long period of time (Skalska et al., 2015; Wang et al., 2008), which affects memory and learning behavior (Mohammadipour et al., 2014; Ze et al., 2014a). The accumulation level and half-life of NPs in CNS are size-dependent (Lee et al., 2013; Park et al., 2010; Sharma et al., 2013). Therefore, pre-evaluating the potential hazards of AgNPs and TiO_2NPs on CNS is necessary.

Pathways of NPs entering the brain are usually divided in two ways: via olfactory nerve or blood-brain barrier (BBB) penetration. BBB is an important structure between the CNS and circulatory system in the brain, which are composed of endothelial cells, basal lamina, astrocyte end feet and pericytes. Endothelial cells, the core anatomical element of BBB, have continuous intercellular tight junctions to reduce transport of substances by the paracellular pathway. Tight junction proteins are classified into two different protein groups: transmembrane proteins (*e.g.*, occludin,

Abbreviations: Ag^+, silver ions; BBB, blood-brain barrier; TiO_2NPs, titanium dioxide nanoparticles; AgNPs, silver nanoparticles; LPS, lipopolysaccharide; ROS, reactive oxygen species; TEER, transendothelial electrical resistance; CNS, central nervous system; ZO, zonula occludens; GLUT-1, glucose transporter; ABC, ATP-binding cassette; FI, fluorescence intensity; DCFH-DA 2′, 7′-dichlorofluorescin diacetate; BSA, bovine serum albumin; DLS, dynamic laser scattering; TEM, transmission electron microscopy; RT, room temperature.

* Corresponding authors.
E-mail addresses: ejchen00@gmail.com (I.-C. Chen), ilunshiou@gmail.com (I.-L. Hsiao), photorice2@gmail.com (H.-C. Lin), chwu@mx.nthu.edu.tw (C.-H. Wu), cychuang@mx.nthu.edu.tw (C.-Y. Chuang), yjhuang@mx.nthu.edu.tw (Y.-J. Huang).

http://dx.doi.org/10.1016/j.etap.2016.09.009
1382-6689/

claudin, junctional adhesion molecules) and peripheral proteins (*e.g.*, zonula occludens (ZO), cingulin). Both types of proteins seal the intercellular cleft, thus preventing free ion diffusion (Shin et al., 2006). Astrocyte end feet almost completely cover the surface of endothelium, and have many specific transport systems, such as ATP-binding cassette (ABC) transporters. The interaction between endothelial cells and astrocytes helps to modulate BBB function (Abbott et al., 2006). The main functions of the BBB are to serve as a guard to select solute, act as carrier to transport nutrients to the brain and remove metabolites from the brain. Even though *in vivo* studies have indicated that silver can be detected in the brain, arguments about whether silver really penetrates BBB and reaches neuron cells, or just accumulates in the endothelial cells is still unknown (Lin et al., 2015). Thus, establishing an *in vitro* BBB model to pre-screen the potential ability and mechanism of NPs to penetrate BBB is important.

One report has indicated that TiO_2NPs can pass through *in vitro* BBB (containing rat primary endothelial and glial cells), and cause BBB dysfunction (Brun et al., 2012). Similarly, AgNPs induce monolayer BBB inflammation by increasing oxidative stress and barrier permeability due to their small size, special modification and high exposure (Cramer, 2014; Trickler et al., 2010). However, these studies only used monolayer endothelial cells or co-culture of endothelial cells and astrocytes in insert and well bottom of Transwell® respectively, which is insufficient to mimic real BBB function and tightness. Moreover, these studies used substitute markers to evaluate the permeability of BBB, and neither quantify how much NPs penetrate BBB nor the amount of NP translocation from endothelial cells to astrocytes. In addition, it is still not clear whether the Ag^+ released from AgNPs or both (AgNPs and Ag^+) contributed the cytotoxicity in BBB. Eventually, neuro-inflammation occurs following almost all CNS pathologies, it is also crucial to understand if more NPs penetrate BBB under inflammatory state.

In this study, endothelial cells and astrocyte-like cells were cultured on different sides of a Transwell insert to mimic the BBB in the brain for evaluating potential hazard of AgNPs and TiO_2NPs on CNS under the pre-inflammatory condition resulting in lipopolysaccharide (LPS). This BBB model has been developed for drug delivery studies (Li et al., 2010), and is useful to observe the influence of elements on the neurovascular unit and the effect of nanotoxicity with cell-to-cell interaction (Naik and Cucullo, 2012; Wilhelm and Krizbai, 2014). After NPs exposure in endothelial cells, the integrity and permeability of BBB was evaluated by detecting the transendothelial electrical resistance (TEER) level, NP concentration in medium and cells, and tight junction protein expression ZO-1 and claudin-5. The cytotoxic effect of NPs as well as ions in BBB model was examined by cell viability, uptake potential, intracellular reactive oxygen species (ROS), and 23 kinds of cytokine secretion.

2. Materials and methods

2.1. NPs and silver ions

AgNPs were supplied by Gold NanoTech, Taipei, Taiwan, were produced by physical manufacturing, and contained no surface modifiers or stabilizers (Hsiao et al., 2015). A silver nitrate ($AgNO_3$) (Sigma-Aldrich, St. Louis) was used as a source of Ag^+ ions. Small- and large-sized TiO_2NPs (TiO_2NPs-S and TiO_2NPs-L) (ST-01, ST-21) (100% anatase, Ishihara Corporation, Japan) has been modified with alkaline solution to increase dispersity (Wu et al., 2016). Procedures were stated in Supporting information. Before characterizing NPs in water or cell medium, stock solutions of NPs were first ultrasonicated at 400W for 10 min (DC400H, DELTA new instrument Ltd., Taiwan) at 25 °C to achieve optimal dispersion. The NPs were characterized for shape/diameter by transmission electron microscopy (TEM, TECNAI 20, Philips, USA), crystal structure by X-ray diffraction analysis (XRD), concentration by inductively coupled plasma optical emission spectrometry (ICP-OES, Agilent 725, USA), and hydrodynamic diameter/zeta potential by Zetasizer Nano ZS (Malvern Instruments Inc., UK).

2.2. Cell culture

Murine brain astrocyte-like cells (ALT, BCRC-60581) were provided by Professor Chi-Shiun Chiang (Cancer Gene Therapy Laboratory, National Tsing Hua University, Hsin-Chu, Taiwan), sourced from *Mus musculus* mouse brain astrocytes with large-T antigen plasmid. Immortalized mouse cerebral endothelial cells (bEnd.3, BCRC-60515) were purchased from the Bioresource Collection and Research Center (Hsin-Chu, Taiwan). Both of the cells were cultured in DMEM supplemented with 10% fetal bovine serum (FBS) and 1% penicillin and streptomycin mixture, and were cultivated in T75 flasks at 37 °C in a humidified atmosphere of 5% CO_2/95% air.

2.3. Establishment of in vitro BBB model

The description of the experimental procedure for building up the *in vitro* BBB model according to (Li et al., 2010). First of all, the bottom side of the Transwell filters (0.4 μm pore sizes, PET, 6 or 12 well; Corning, USA) were coated with collagen type I (8 μg/cm^2 in 0.02 N acetic acid) for 1 h at room temperature (RT) to help cell attachment. Then, the filters were washed with 1 × phosphate-buffered saline (PBS), and ALT cells were seeded onto the back of the Transwell filters at a density of 2.44×10^4 cells/cm^2. After 3 h incubation, bEnd.3 cells were seeded onto the top side of the filters at a density of 10^5 cells/cm^2 and co-cultured with ALT cells for 4 days.

2.4. Exposure condition and dosages of NPs

After 4 days, both chambers were pre-treated w/or w/o LPS (2 μg/mL) from *Escherichia coli* 055:B5 (Sigma-Aldrich, St. Louis) in serum-free DMEM medium for 6 h. Then, the same volume of NPs or Ag^+ suspensions as pre-treatment were added to the top chamber of Transwell to achieve final concentration of LPS (1 μg/mL), TiO_2NPs (100 ppm), AgNPs (4 ppm) and Ag^+ (1.8 ppm) in DMEM/10%FBS medium for 24 h incubation.

2.5. Cell viability

AlamarBlue® (AbD Serotec, Kidlington, UK) as a cell viability indicator was used in monoculture testing. Briefly, after 24 h NP exposure, the alamarBlue® reagent was mixed 1:10 to DMEM/10%FBS followed by a 2 h incubation at 37 °C. Results of cell viability were determined by fluorescence at excitation wavelengths of 530 nm with emission at 590 nm. Cell viability was calculated using the expression (fluorescence intensity (FI) of test agent)/(FI of untreated control) × 100. Cell viability in BBB model was evaluated by flow cytometry (FACSCanto II, BD Biosciences, USA) with 10,000 cells collected, using a propidium iodide (PI) reagent. After NPs exposure for 24 h, the solution of both top and bottom chambers was aspirated to another plate for cytokines analysis, and then the cells were collected for PI staining (40 μg/mL). The dead cells were detected by flow cytometry. Cell viability was calculated using 100-(percentage of dead cell)%.

2.6. Cell uptake potential

After LPS and NPs treatment, the cells were collected and analyzed by flow cytometry. Potential cell uptake of NPs by flow

cytometry light scatter analysis was developed by Suzuki et al. (Suzuki et al., 2007). Evaluation of SSC intensity was carried out using a flow cytometry (BD Biosciences), and data were analyzed using Flowing Software 2. The amounts of particles taken up by the cells were analyzed using geometric mean of SSC intensity.

2.7. Intercellular ROS generation

Intracellular ROS production was measured using 2′,7′-dichlorofluorescin diacetate (DCFH-DA, Sigma-Aldrich as a reactive fluorescent probe. After NPs exposure for 24 h, the solutions were discarded, and these cells were washed once by PBS. After that, cells were harvested and incubated with 10 μM DCFH-DA in non-phenol red DMEM at 37 °C for 30 min. The solutions were then centrifuged (200*g*, 5 min) and the supernatant medium removed entirely. Prior to measurement, the cells were re-suspended in PBS. The fluorescence was determined using flow cytometry, with 10,000 cells collected. The fluorescence was detected at 528 nm after excitation at 488 nm. The geometric mean fluorescence intensity was analyzed using Flowing Software 2.

2.8. Cytokine secretion

The suspension of top and bottom chambers in BBB model was collected and 23 kinds of cytokines (IL-1α, IL-1β, IL-2, IL-4, IL-5, IL-6, IL-9, IL-10, IL-12(p40), IL-12(p70), IL-13, IL-17, Eotaxin, G-CSF, GM-CSF, IFN-γ, KC, MCP-1, MIP-1α, MIP-1β, RANTES, TNF-α) were detected using Bio-Plex Multiplex assay (Yu-shing Biotech. Ltd., Taiwan). Briefly, selected coupled beads were added to a 96-well plate and incubated for 30 min. Next, biotin-labeled detection antibodies were added to wells and incubated for 30 min. Then, a fluorescently labeled streptavidin reporter was added to wells for 10 min to bind biotin-labeled detection antibodies, and were measured with a Bio-Plex® 200 Multiplex reader.

2.9. TEER determination

TEER is a preliminary and simple way for a Transwell system to assess *in vitro* BBB integrity. After LPS treatment, NPs and Ag^+ in the *in vitro* BBB, TEER values were determined by Millicell® ERS-2 (Millipore, USA). Prior to use, the functionality was calibrated. The STX01 electrodes were then sterilized by 70% ethanol. Before measurements, the electrodes were rinsed by culture medium and then put into both Transwell chambers. The results were corrected by blanks, and the resistance was multiplied by the effective surface area of the filter membrane. The unit would express in Ω cm^2 (Buchert et al., 2012).

$$R_{sample} - R_{blank} = R$$

$$\text{Unit area resistance} = \text{Resistance}(\Omega) \times \text{Effective membrane area}(cm^2)$$

2.10. Immunofluorescence staining of tight junction

Tight junction protein expression contributing to strong blood-brain barrier resistance was comfirmed by immunofluorescence assay. After TEER determination, cells on Transwell inserts were washed once with PBS, and fixed with 4% paraformaldehyde. Then, they were permeabilized with 1% Triton X-100 in PBS for 10 min at RT. Next, the inserts were blocked with 3% bovine serum albumin (BSA) in PBS for 30 min at RT. After PBS washing, the primary antibodies of ZO-1 (ZO-1 rabbit polyclonal antibody, Invitrogen) or claudin-5 (claudin-5 rabbit polyclonal antibody, Invitrogen) were diluted in 3% BSA/PBS at 1:100, and applied for 1 h at RT. The inserts were then washed with PBS three times, and incubated in the dark with Alexa Fluor 488 goat anti-rabbit IgG (H + L) secondary antibodies (1:200 in PBS, Molecular Probes, Thermo Fisher Scientific, USA) for 1 h at RT. Finally, the inserts were washed with PBS 3–5 times, and the membrane of the inserts were cut off and mounted in antifade mountant solution with DAPI (ProLong® diamond antifade mountant with DAPI, Molecular Probes, Thermo Fisher Scientific). The images were obtained by Nikon ECLIPSE T*i*-U microscope with a 60 × oil-immersion objective using 488 nm laser for Alexa-488.

2.11. Permeability coefficient

In order to calculate the permeability, the medium and cells from both the top and bottom sides of the BBB model was collected and the NP concentration was measured by inductively coupled plasma-mass spectrometer (ICP-MS). Samples were acidified with 65% HNO_3 for AgNPs or 1:2 65% HNO_3 and 5% HF in volume for TiO_2NPs. Suspensions were then digested at 70 °C for 24 h and filled de-ionized water to 15 mL before analysis. ^{107}Ag, ^{47}Ti analysis was conducted using a quadrupole ICP mass spectrometer (Agilent 7500a, USA). The transportation capacity was evaluated by permeability coefficient (P (Yuan, 2010), P′, or P″), which is calculated by following equation:

$$P = \frac{\text{Bottom chamber concentration}}{t} \times \frac{1}{A} \times \frac{V_{bottom}}{\text{Top chamber concentration}}$$

$$P' = \frac{\text{NPs concentration in ALT cells}}{t} \times \frac{1}{A} \times \frac{V_{bottom}}{\text{NPs concentration in bEnd.3 cells}}$$

$$P'' = \frac{\text{Bottom chamber concentration with ALT cells}}{t} \times \frac{1}{A} \times \frac{V_{bottom}}{\text{Top chamber concentration with bEnd.3 cells}}$$

t: time (24 h); A: surface area of membrane (for 6 well is 4.67 cm^2); V: medium volume in bottom side; All concentrations were subtracted the background control groups without NPs.

2.12. Statistics

Significant differences between treatment groups and control/LPS-only group were analyzed by one-way analysis of variance (ANOVA) followed by Dunnett's multiple comparison post-tests. The statistical differences between two experimental groups were analyzed by Student's unpaired *t*-test. P values < 0.05 were considered significant.

3. Results and discussion

3.1. Characterization of NPs

The size and morphology of NPs were observed by TEM. Size of AgNPs, TiO_2NPs-S and TiO_2NPs-L were 8.4 nm, 6 nm and 35.1 nm in geometric mean diameter, respectively (Fig. S1). Hydrodynamic diameters of NPs in deionized water and culture medium, measured by dynamic light scattering (DLS), were 114.5 ± 2.8 nm and 105.6 ± 20.2 nm for AgNPs; 48.4 ± 2.0 nm and 91.5 ± 2.3 nm for TiO_2NPs-S and 130.5 ± 2.1 nm and 244.6 ± 11.8 nm for TiO_2NPs-L. The AgNPs and TiO_2NPs-S have almost the same secondary size in medium. The DLS size of three NPs in medium did not change after 24 h, which had a good stability (data not shown). The zeta potential of AgNPs was 6.3 mV in deionized water and −5.5 mV in culture medium. For TiO_2NPs-S and TiO_2NPs-L, the zeta potential was 44 and 42.8 mV in deionized water and −14.4 and −9.9 mV in culture medium (Tables S1). The different sizes and surface charges of NPs

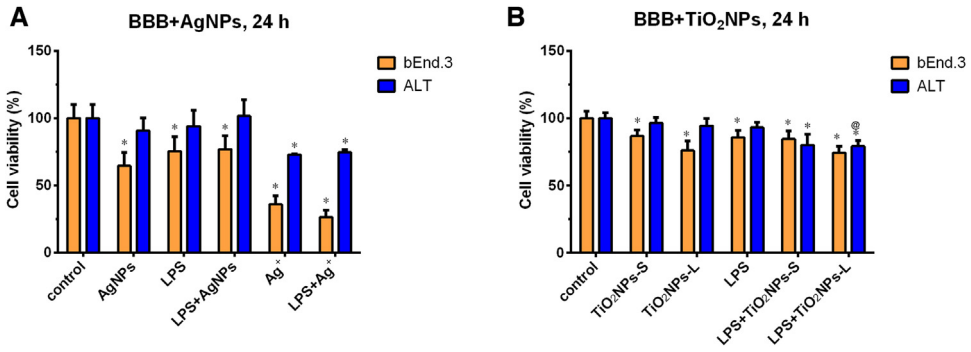

Fig. 1. Cell viability of bEnd.3 and ALT cells in BBB model system. (A) 24 h after treatment with 4 ppm AgNPs and 1.8 ppm Ag^+, or co-treatment without or with LPS. (B) 24 h after treatment with 100 ppm TiO_2NPs-S and TiO_2NPs-L, or co-treatment without or with LPS. * and @ indicate that cell viability differed significantly from control without LPS and with LPS groups, respectively, with P-value < 0.05.

in water and medium can be related to adsorption of negative-charged protein corona and/or AgNP dissolution (Eudald et al., 2011; Hsiao et al., 2015; Murdock et al., 2008).

3.2. Cell viability of bEnd.3 and ALT cells in BBB model

Comparing the cell viability with treatment of AgNPs and TiO_2NPs to the two kinds of cells in a mono-culture system, we found that in the same size, AgNPs were more toxic than TiO_2NPs-S; there was no cytotoxicity after 15 ppm TiO_2NPs-S exposure to ALT cells or bEnd.3 cells, while lower concentration of AgNPs (2 ppm) caused significant viability loss in two cell lines (Figs. S2). Similar to our study, Trickler et al. found that the cell viability of rat brain microvessel endothelial cells (rBMEC) decreases approximately 70% after exposure to 25 ppm AgNPs (25 nm or 40 nm) (Trickler et al., 2010). Moreover, exposure of endothelial cells to 21 nm TiO_2NPs decreases cell viability at high concentration (235 ppm) (Halamoda Kenzaoui et al., 2012; Hou et al., 2014).

To figure out the two kinds of NPs in BBB integrity and permeability, 4 ppm AgNPs and 100 ppm TiO_2NPs under the similar cell viability basis (75% for bEnd.3 cells and 60% for ALT cells from monoculture results; Fig. S2) were selected for the exposure dose in BBB model. On the other hand, 1.8 ppm Ag^+ is determined by the soluble silver content in the AgNP (45% AgNP dissolution rate in culture medium at 24 h (Hsiao et al., 2015)). The strategy was also the same as a previous report (van der Zande et al., 2012).

After treatment of AgNPs, the viability of bEnd.3 cells in BBB decreased, but ALT cells were not affected (Fig. 1A). There was similar effect of both TiO_2NPs-S and TiO_2NPs-L to AgNPs on the BBB (Fig. 1B). Because endothelial cells are the first line of defense against outer substances attacking the CNS, bEnd.3 cells are like security guards against damage from NPs and for protecting ALT cells. However, the viability of both bEnd.3 cells and ALT cells were significant decreased after Ag^+ exposure (Fig. 1A). This suggested that Ag^+ is more toxic than AgNPs to BBB. This observation is in agreement with an *in vitro* study that compared the toxicity of two forms silver in rat cerebral astrocytes (Sun et al., 2016). There was no significant difference of viabilities in bEnd.3 cell by two sizes of TiO_2NPs. Although smaller TiO_2NPs-S has higher surface area and suspension stability than TiO_2NPs-L, a rapid sedimentation rate of large TiO_2NPs-L may cause similar cell-NP interaction between two particles. On the other hand, when BBB model with LPS treatment, the viability in bEnd.3 cells was decreased but not in ALT cells. However, ALT cells were injured when co-treated with LPS and TiO_2NPs for 24 h (Fig. 1B).

3.3. Uptake potential and quantification of NPs in BBB model

The update potential of ALT cells and bEnd.3 cells was determined. In mono-culture system, both ALT cells and bEnd.3 cells were observed to have higher potential to uptake AgNPs and TiO_2NPs (Fig. S3). In BBB model, AgNPs can not be detected after 24 h exposure in bEnd.3 cells and ALT cells by flow cytometry (Fig. 2A); nevertheless, silver was detected in both cell layers by high sensitive ICP-MS (Fig. 2C). With the treatment of AgNPs, more silver were detected in bEnd.3 cell layer than that in ALT layer. By contrast, an opposite result was found in co-treatment of LPS (Fig. 2C). Less silver was detected in bEnd.3 cells and ALT cells with the treatment of Ag^+ than AgNPs treatment, especially in ALT layer (Fig. 2C). Our previous and other studies have demonstrated that Ag ions uptake ratio of cells (including ALT cells) is significantly lower than that of AgNPs due to membrane barrier (Cronholm et al., 2013; Hsiao et al., 2015).

On the other hand, Fig. 2B illustrated that single bEnd.3 cells had the high potential to uptake TiO_2NPs-S and TiO_2NPs-L. However, the uptake of TiO_2NPs-S and TiO_2NPs-L was not found in single ALT cells no matter w/or w/o LPS treatment. A similar result was also observed from ICP-MS determination (Fig. 2D). These results indicated that bEnd.3 did prevent most TiO_2NPs from passing through BBB. Ye et al. (Ye et al., 2015) presented that AuNPs and SiO_2NPs are accumulated in a monolayer hCMEC/D3 endothelial BBB model using TEM images, and were transported by endo-lysosomal pathway. Moreover, TEM images from Brun et al. (Brun et al., 2012) showed that TiO_2NPs are taken into endothelial cells and transported to the glial cells in the well bottom. According to our observations, NPs not only accumulated in BBB but also performed the probability of passing through the BBB potentially to injury the CNS.

3.4. Intercellular ROS generation

Studies have revealed that AgNPs and TiO_2NPs can induce ROS generation. Shi et al. (Shi et al., 2014) revealed that the AgNPs lead to ROS generation and influence human umbilical vein endothelial cells (HUVECs). TiO_2 induces ROS production in HUVECs at 5 and 20 $\mu g/cm^2$ (Montiel-Davalos et al., 2012). This was consistent with our results in mono-culture system that AgNPs and TiO_2NPs induced ROS in bEnd.3 cells and ALT cells (Fig. S4).

Different from mono-culture system, when exposure to AgNPs w/or w/o LPS, the intracellular ROS of BBB model was significantly increased in bEnd.3 cells but not in ALT cells (Fig. 3A). Ag^+ exposure did not induce ROS release from both cells, while co-treatment of LPS induced more ROS than LPS-only group in bEnd.3 cells. When exposure to TiO_2NPs-S and TiO_2NPs-L w/or w/o LPS, no any increase

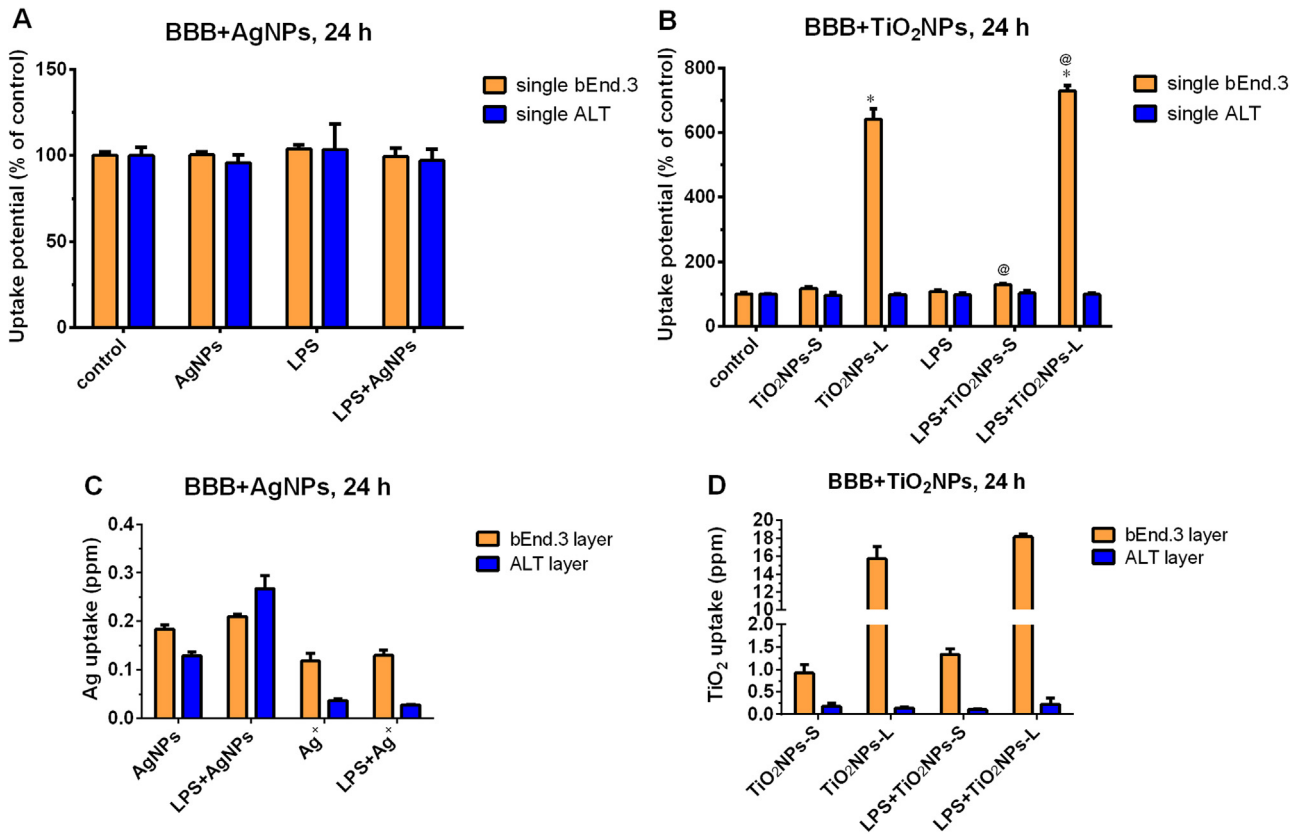

Fig. 2. Uptake potential (A)(B) and uptake quantification (C)(D) of NPs in bEnd.3 and ALT cells of BBB. (C) cellular uptake quantification of AgNPs and Ag^+ −treated BBB. * and @ indicate that the uptake potential differed significantly from control without LPS and with LPS groups, with P-value < 0.05.

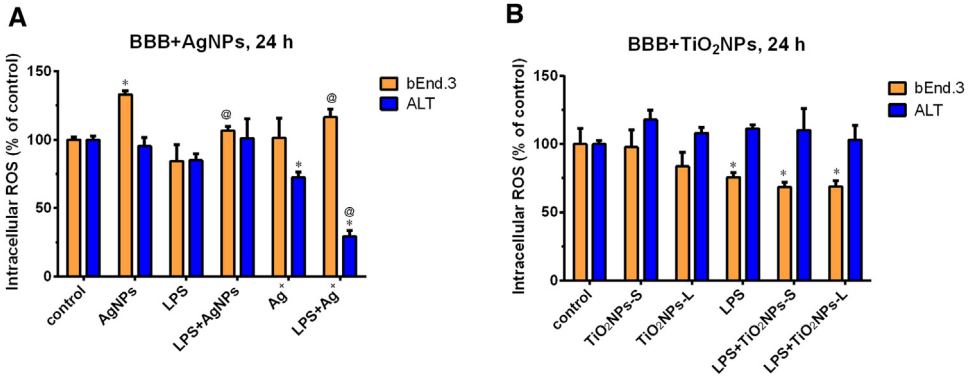

Fig. 3. Intercellular ROS generation of bEnd.3 and ALT cells of BBB. (A) 24 h after treatment with 4 ppm AgNPs and 1.8 ppm Ag^+, or co-treatment without or with LPS. (B) 24 h after treatment with 100 ppm TiO_2NPs-S and TiO_2NPs-L, or co-treatment without or with LPS.* and @ indicate that ROS differed significantly from control without LPS and with LPS groups, respectively, with P-value < 0.05.

of ROS than control group in both bEnd.3 cells and ALT cells (Fig. 3B). Sun et al. (Sun et al., 2016) presented PVP-coated AgNPs (1 μg/mL 24 nm) causes elevated ROS within 24 h in rat primary astrocytes, while Ag^+ (0.1 μg/mL) does not. Onodera et al. (Onodera et al., 2015) found that AgNPs (1 nm and 70 nm) can induce ROS in BALB/3T3 cells within 1 h, but Ag^+ (5 μg/mL) can not. These studies indicated that toxic potency of AgNPs to BBB differed from Ag^+.

3.5. Cytokines secretion

As unbalanced level of ROS leads to enhance oxidative stress and stimulate inflammatory response (Song et al., 2014), the secretion of cytokines after AgNPs or Ag^+ exposure were determined. Interestingly, Ag^+ exposure significantly induced IL-2, IL-4, IL-12, IL-13, IFN-γ and TNF-α but no significant cytokine secretion was found after AgNP exposure, which induced ROS in bEnd.3 cells (Fig. 4A, C). Trickler et al. (Trickler et al., 2010) reported that PVP-coated AgNPs (25 nm) induced IL-1β, TNF and PGE2 in primary rat brain microvessel endothelial cells. Sun et al. (Sun et al., 2016) also found PVP-coated AgNPs (24 nm) induced CINC-2α/β, CINC-3, fratalkine, IL-10, IP-10, L-selectin and thymus chemokine in rat primary astrocytes. The reasons of the results of this study different from previous studies might be the different use of cell models and surface-functionalized AgNPs or the release of cytokines was not analyzed in our study.

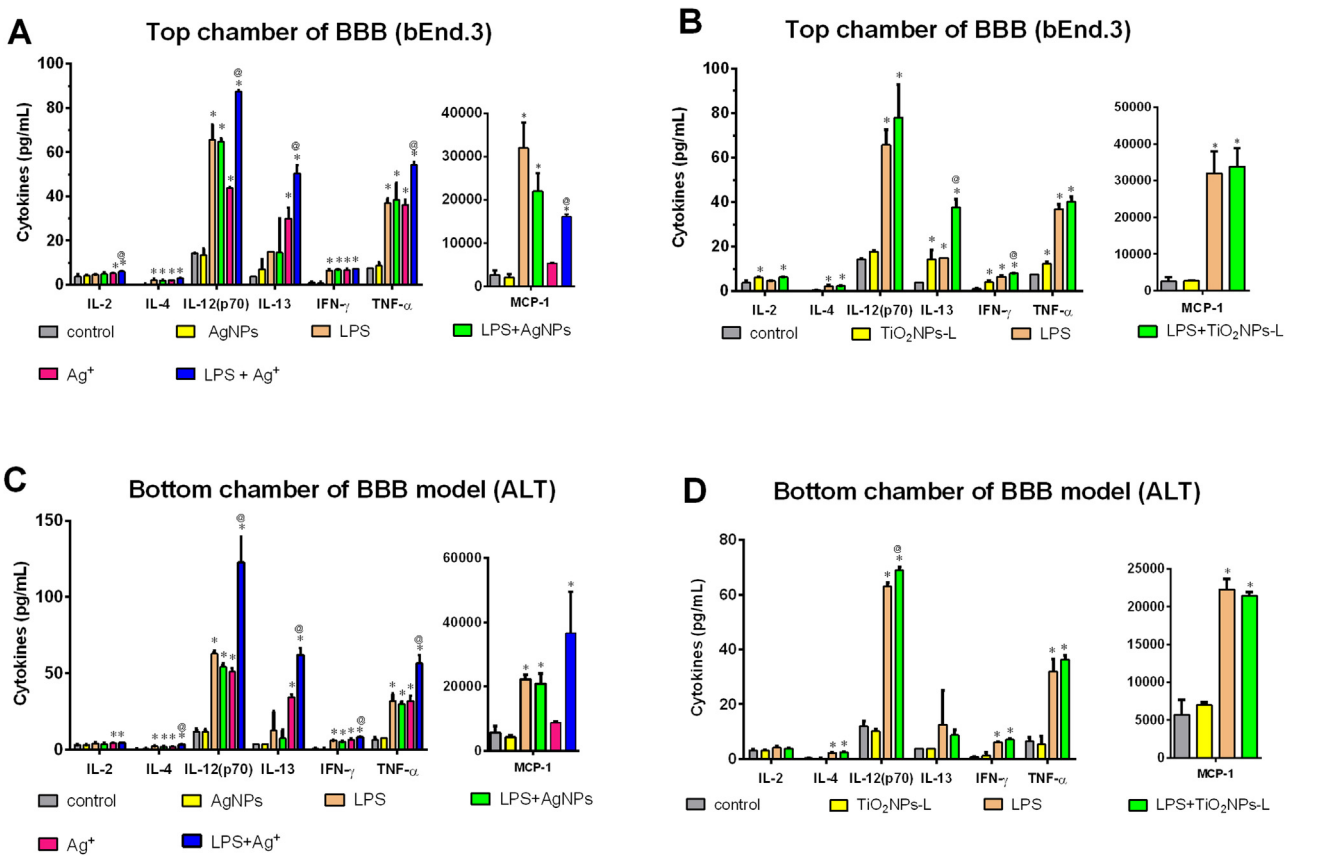

Fig. 4. Cytokines secretion from top or bottom chamber of BBB model. (A) and (C) show cytokines release from top/bottom chambers after 24 h, 4 ppm AgNPs and 1.8 ppm Ag^+ exposure. (B) and (D) show cytokines secreted from top/bottom chambers after 24 h 100 ppm TiO_2NPs-L exposure. * and @ indicate that cytokine secretion differed significantly from control without LPS and with LPS, respectively, with P-value < 0.05.

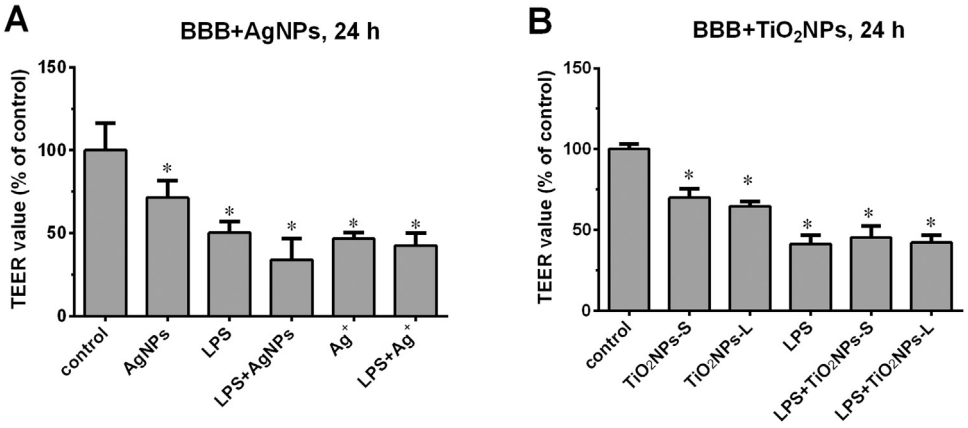

Fig. 5. TEER values of BBB model. (A) 24 h after treatment with 4 ppm AgNPs and 1.8 ppm Ag^+, or co-treatment without or with LPS. (B) 24 h after treatment with 100 ppm TiO_2NPs-S and TiO_2NPs-L, or co-treatment without or with LPS. * and @ indicate that TEER value differed significantly from control without LPS and with LPS, respectively, with P-value < 0.05.

Fig. 4A and C showed that IL-4, IL-12, IFN-γ, TNF-α and MCP-1 were detected in both chambers of the BBB model. Co-treatment of AgNPs with LPS did not promote pro-inflammatory cytokines to release. However, co-treatment of Ag^+ with LPS stimulated 7 kinds of cytokines to release. These evidences supported again that toxic potency of AgNPs to BBB differed from Ag^+.

Fig. 4B showed that IL-2, IL-13, IFN-γ and TNF-α were significantly secreted in the top chamber (bEnd.3 cells) after exposure to TiO_2NPs-L without LPS. Comparing with LPS-only group, IL-13, IFN-γ, IL-12 significantly increased from top and bottom chamber (IL-12) respectively after co-treatment of LPS and TiO_2NPs. Reports have found that IFN-γ stimulated ROS from microglia and astrocytes, enhanced vascular permeability and also promoted TNF-α and IL-1 production (Abbas et al., 2002; Chuang et al., 2015; Sheng et al., 2013). IL-12 not only stimulates the production of IFN-γ and TNF-α, but also reduces anti-inflammation marker IL-4-mediated inhibition of IFN-γ (Gately et al., 1994). TNF-α has been found to promote BBB disruption (Dong and Benveniste, 2001). Therefore, the decrease of cell viability in ALT cells of BBB as LPS co-treatment with TiO_2NPs or Ag^+ (w/or w/o LPS) could be partially due to the cytokine secretion *e.g.*, TNF-α caused apoptosis of ALT cells.

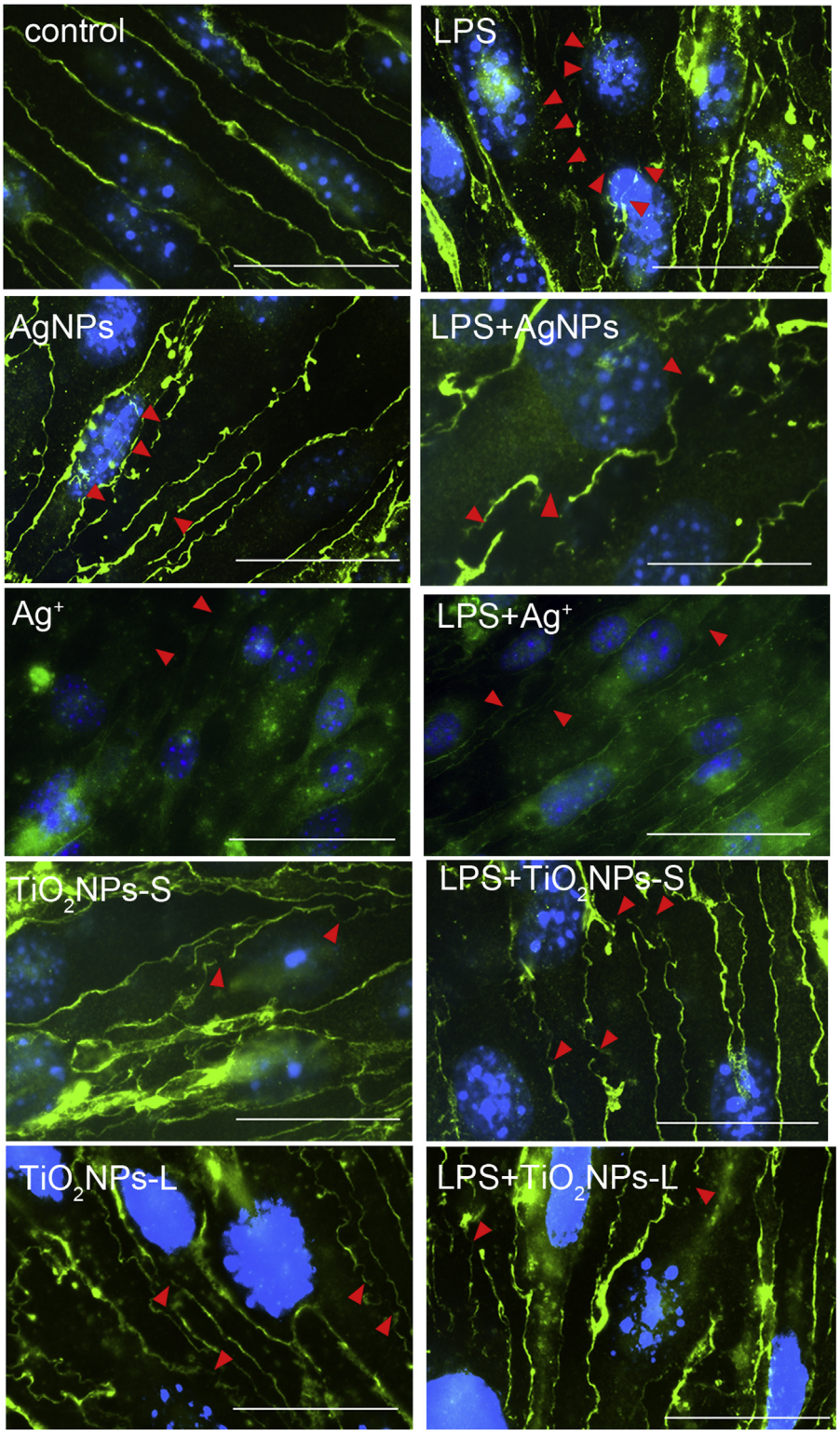

Fig. 6. The expression of tight junction protein ZO-1 in BBB model. Red triangles: the interrupted lines. Green: ZO-1 proteins; Blue: cell nucleus. (For interpretation of the references to colour in this figure legend, the reader is referred to the web version of this article.)

3.6. TEER measurement

TEER is a preliminary and simple way in a Transwell system to assess the extent of BBB integrity. A high resistance value indicates that the structure of the BBB has integrity and tightness. In contrast, a low resistance value indicates that the structure of BBB is damaged and highly permeable. We found that the TEER value of the BBB decreased after exposure to AgNPs, Ag^+ and both TiO_2NPs-S or TiO_2NPs-L (Fig. 5). Ag^+ caused more significant decrease of TEER value than AgNPs. LPS itself reduced the TEER value dramatically. Co-treatment of LPS with AgNPs or Ag^+ did not reduce more TEER value. Co-treatment of LPS with TiO_2NPs did not cause lower TEER

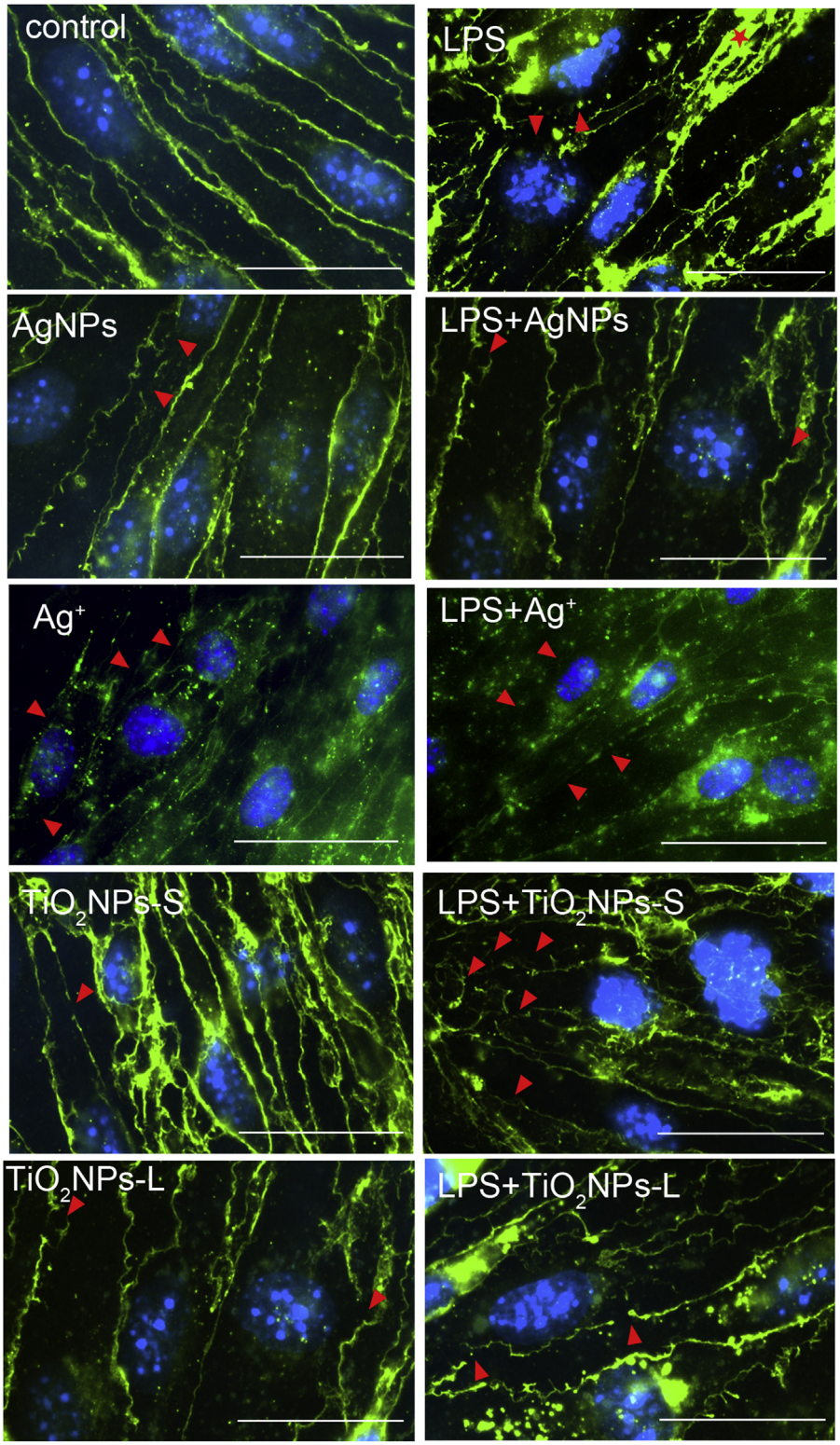

Fig. 7. The expression of tight junction protein claudin-5 in BBB model. Red triangles indicate the interrupted lines and stars represent the spread of claudin-5 to cytoplasm. Green: claudin-5 proteins; Blue: cell nucleus. (For interpretation of the references to colour in this figure legend, the reader is referred to the web version of this article.)

value than LPS-only group. Different size of TiO_2NPs also did not affect significant differences on TEER value.

3.7. *Immunofluorescence staining of tight junction protein*

In order to further verify the disruption of BBB structure, the variation of tight junction proteins claudin-5 and ZO-1 was observed. Claudin-5 is one of the major claudin proteins in brain endothelial cells that allow small molecules (<800 Da) to pass through, as well as regulates paracellular ions and size selectivity (Nitta et al., 2003; Van Itallie et al., 2001). ZO-1 is one of the peripheral proteins that links transmembrane proteins and cytoskeleton, and also participate in cell signal activation.

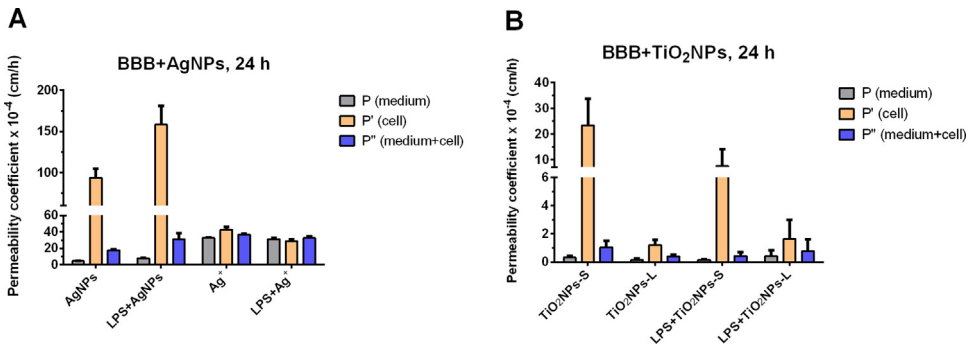

Fig. 8. Permeability coefficient of NPs in BBB model. (A) AgNPs and Ag^+; (B) TiO_2NPs. The AgNPs, Ag^+ and TiO_2NPs were actually transported from top side (*i.e.*, circulatory system) to bottom side (*i.e.*, central nervous system) with different capability.

The ZO-1 and claudin-5 images in the control of the BBB appeared as continuous fluorescent lines (Figs. 6, 7). Non-continuous lines of the ZO-1 staining after AgNPs exposure were shown in Fig. 6. Claudin-5 appeared more disordered or with interrupted lines after AgNPs exposure (Fig. 7). Loss of ZO-1 and claudin-5 lines after Ag^+ exposure was observed (Figs. 6, 7), which corresponded to the TEER and cell viability results. Regarding exposure to TiO_2NPs-S and TiO_2NPs-L, tight junction proteins (ZO-1, claudin-5) were also disrupted. Corresponding to TEER results, different sizes of TiO_2NPs w/or w/o LPS did not cause different levels of disruption on ZO-1 and claudin-5. LPS itself caused severe disruption of continuous ZO-1 and claudin-5 express (Figs. 6, 7). When AgNPs were co-treated with LPS, more severe disruption on ZO-1 and claudin-5 tight junction proteins was observed compared to the LPS-only group (Figs. 6, 7) as well as in TiO_2NPs co-treatment group.

The BBB breakdown may relate to ROS, inflammatory cytokines, leukocyte adhesion and so forth (Obermeier et al., 2013). Regarding data in BBB system (Fig. 3), AgNPs induced high levels of ROS generation from bEnd.3 cells, which might result in tight junction proteins disruption (Zehendner et al., 2013), and TEER value decrease. Ag^+ and TiO_2NPs did not induce ROS while both induced significant secretion of cytokines including TNF-α, IL-13 and IFN-γ (Fig. 4), which may participate in BBB breakdown. In addition, the low viability of endothelial cells and astrocytes after NPs or ion exposure also caused the discontinuous tight junction proteins due to fewer cells leading to a weakened BBB structure.

LPS induced a high level of secretion in IL-4, IL-12, IL-13, MCP-1, TNF-α and IFN-γ. Other reports also found that LPS induces many kinds of cytokines and also disrupts ZO-1 or claudin-5 expression (He et al., 2011; Seok et al., 2013). In these cytokines, MCP-1 is demonstrated to cause BBB breakdown and hyperpermeability (Stamatovic et al., 2003). Additionally, TNF-α and IFN-γ can increase BBB permeability and be related to neurodegenerative diseases (Capaldo and Nusrat, 2009; Deli et al., 1995). Thus, those inflammatory cytokines induced by LPS influenced the integrity of the BBB to result in the decreased TEER values. Co-treatment of Ag^+ with LPS released more cytokines and thus caused more severe BBB disruption.

3.8. Permeability coefficient

Most studies did not directly determine the amount of transported NPs, instead of adding fluorescein or radio labelled markers, such as FITC-Dextrane or ^{14}C-sucrose to detect the permeability (Cramer, 2014; Trickler et al., 2010). Thus, in order to know the actual amount of AgNPs that would pass in BBB model, we modified the research of Hanada et al. (Hanada et al., 2014) that directly detect the fluorescence intensity of fluorescent particles to quantify NPs by ICP-MS. Using this method, we can observe that NPs were actually transported from the luminal side (*i.e.*, circulatory system) to the abluminal side (*i.e.*, central nervous system) that indicated NPs able to penetrate BBB.

In this study, three kinds of permeability coefficient were calculated and discussed. Permeability coefficient P represented the capacity of NPs to pass through BBB, permeability coefficient P' represented the ratio of NPs to transport from bEnd.3 cells to ALT cells, and another permeability coefficient P" represented the whole movement of NPs in BBB model.

Fig. 8 revealed the permeability coefficients P, P', P" of Ag^+, AgNPs and TiO_2NPs. Ag^+ had higher P value and lower P' value than AgNPs, which meant silver ions have higher BBB penetration while lower cell translocation than AgNPs. Ag^+ caused high toxicity to bEnd.3 cells and ALT cells, which was reasonably easier to penetrate already-disrupted BBB than AgNPs. However, Ag^+ was not easy to be taken into the cells due to membrane barrier, which presented a lower P' value than AgNPs.

When co-treatment with AgNPs and LPS, the permeability coefficients P, P', P" were enhanced, which was because co-treatment of AgNPs and LPS disrupted BBB more serious. Moreover, permeability coefficients values of AgNPs w/or w/o LPS were significantly higher than that of small sized TiO_2NPs-S w/or w/o LPS (Fig. 8). These suggested that AgNPs can pass through BBB model easily to the bottom chamber with fewer remaining in the cells. On the other hand, TiO_2NPs had lower translocation ratio from bEnd.3 cells to ALT cells, and thus fewer passed through to arrive in the bottom chamber. A main possible reason of high BBB penetration capability for AgNPs was dissolution of AgNPs to Ag ions in medium (Hsiao et al., 2015). Furthermore, our previous study has demonstrated that LPS did not affect AgNP dissolution in medium (Hsiao et al., 2015), which can neglect Ag ion factor in promoting BBB disruption when co-treatment of AgNPs and LPS.

Small sized TiO_2NPs-S had higher permeability coefficients than TiO_2NPs-L, which indicated a size-dependent BBB penetration (Fig. 8B). Many studies have also found the same results. For example, TiO_2NPs (10, 20, and 200 nm) were treated rats through aerosol inhalation, while only 10 and 20 nm were both transported into the brain after 72 h (Liu et al., 2013). PEGylated silica NPs (25 nm) were able to migrate across *in vitro* and *in vivo* BBB within 1 h, while not for 50 nm and 100 nm one (Liu et al., 2014).

4. Conclusions

As to the TEER value and ZO-1 and claudin-5 tight junction marker, Ag^+, the different exposure level of AgNPs and TiO_2NPs can damage the BBB integrity, and found the toxic potency of ion and NPs were different. AgNPs-induced BBB disruption was related to ROS-induced cell death. Ag^+ and TiO_2NPs exposure disrupted BBB by cytokine secretion (IL-4, IL-12(p70), IL-13, IFN-γ, and TNF-α)

especially when co-treatment with LPS. Ag^+ led to higher permeability in BBB model while lower cell-to-cell translocation ratio than AgNPs. These evidences indicated that particle-specific effects should also be considered to evaluate the AgNP toxicity in BBB. In the same size, both AgNPs and TiO_2NPs-S actually penetrated *in vitro* BBB, and AgNPs were more efficient than TiO_2NPs, which indicated AgNPs had more probability to cause injury in the CNS. Size-dependent BBB penetration also was observed in TiO_2NPs. The *in vitro* BBB model used in this study offered a simple and quick method for evaluating toxic potency of NPs in CNS system, which is useful for safety design of nanomaterials.

Funding sources

This work was supported by the Ministry of Science and Technology (MOST), Taiwan [103-2221-E-007-006-MY3].

Appendix A. Supplementary data

Supplementary data associated with this article can be found, in the online version, at http://dx.doi.org/10.1016/j.etap.2016.09.009.

References

Abbas, N., Bednar, I., Mix, E., Marie, S., Paterson, D., Ljungberg, A., Morris, C., Winblad, B., Nordberg, A., Zhu, J., 2002. Up-regulation of the inflammatory cytokines IFN-gamma and IL-12 and down-regulation of IL-4 in cerebral cortex regions of APP(SWE) transgenic mice. J. Neuroimmunol. 126, 50–57.

Abbott, N.J., Ronnback, L., Hansson, E., 2006. Astrocyte-endothelial interactions at the blood-brain barrier. Nat. Rev. Neurosci. 7, 41–53.

Brun, E., Carriere, M., Mabondzo, A., 2012. In vitro evidence of dysregulation of blood-brain barrier function after acute and repeated/long-term exposure to TiO(2) nanoparticles. Biomaterials 33, 886–896.

Buchert, M., Turksen, K., Hollande, F., 2012. Methods to examine tight junction physiology in cancer stem cells: TEER, paracellular permeability, and dilution potential measurements. Stem Cell Rev. 8, 1030–1034.

Capaldo, C.T., Nusrat, A., 2009. Cytokine regulation of tight junctions. Biochim. Biophys. Acta 1788, 864–871.

Chuang, D.Y., Simonyi, A., Kotzbauer, P.T., Gu, Z., Sun, G.Y., 2015. Cytosolic phospholipase A2 plays a crucial role in ROS/NO signaling during microglial activation through the lipoxygenase pathway. J. Neuroinflammation 12, 199.

Cramer, S., 2014. The Influence of silver nanoparticles on the blood-brain and the blood-cerebrospinal fluid barrier in vitro. J. Nanomed. Nanotechnol. 05.

Cronholm, P., Karlsson, H.L., Hedberg, J., Lowe, T.A., Winnberg, L., Elihn, K., Wallinder, I.O., Moller, L., 2013. Intracellular uptake and toxicity of Ag and CuO nanoparticles: a comparison between nanoparticles and their corresponding metal ions. Small 9, 970–982.

Deli, M.A., Descamps, L., Dehouck, M.P., Cecchelli, R., Joo, F., Abraham, C.S., Torpier, G., 1995. Exposure of tumor necrosis factor-alpha to luminal membrane of bovine brain capillary endothelial cells cocultured with astrocytes induces a delayed increase of permeability and cytoplasmic stress fiber formation of actin. J. Neurosci. Res. 41, 717–726.

Dong, Y., Benveniste, E.N., 2001. Immune function of astrocytes. Glia 36, 180–190.

Eudald, C., Tobias, P., Albert, D., Gertie, J.O., Víctor, F.P., 2011. Hardening of the nanoparticle?protein corona in metal (Au, Ag) and oxide (Fe_3O_4, CoO, and CeO_2) nanoparticles. Small 7, 3479–3486.

Gately, M.K., Warrier, R.R., Honasoge, S., Carvajal, D.M., Faherty, D.A., Connaughton, S.E., Anderson, T.D., Sarmiento, U., Hubbard, B.R., Murphy, M., 1994. Administration of recombinant IL-12 to normal mice enhances cytolytic lymphocyte activity and induces production of IFN-gamma in vivo. Int. Immunol. 6, 157–167.

Genter, M.B., Newman, N.C., Shertzer, H.G., Ali, S.F., Bolon, B., 2012. Distribution and systemic effects of intranasally administered 25 nm silver nanoparticles in adult mice. Toxicol. Pathol. 40, 1004–1013.

Gupta, S.M., Tripathi, M., 2011. A review of TiO_2 nanoparticles. Chin. Sci. Bull. 56, 1639–1657.

Halamoda Kenzaoui, B., Chapuis Bernasconi, C., Guney-Ayra, S., Juillerat-Jeanneret, L., 2012. Induction of oxidative stress, lysosome activation and autophagy by nanoparticles in human brain-derived endothelial cells. Biochem. J 441, 813–821.

Hanada, S., Fujioka, K., Inoue, Y., Kanaya, F., Manome, Y., Yamamoto, K., 2014. Cell-based in vitro blood-brain barrier model can rapidly evaluate nanoparticles' brain permeability in association with particle size and surface modification. Int. J. Mol. Sci. 15, 1812–1825.

He, F., Peng, J., Deng, X.L., Yang, L.F., Wu, L.W., Zhang, C.L., Yin, F., 2011. RhoA and NF-kappaB are involved in lipopolysaccharide-induced brain microvascular cell line hyperpermeability. Neuroscience 188, 35–47.

Hou, Y., Lai, M., Chen, X., Li, J., Hu, Y., Luo, Z., Ding, X., Cai, K., 2014. Effects of mesoporous SiO_2, Fe_3O_4, and TiO_2 nanoparticles on the biological functions of endothelial cells in vitro. J. Biomed. Mater. Res. A 102, 1726–1736.

Hsiao, I.L., Hsieh, Y.K., Wang, C.F., Chen, I.C., Huang, Y.J., 2015. Trojan-horse mechanism in the cellular uptake of silver nanoparticles verified by direct intra- and extracellular silver speciation analysis. Environ. Sci. Technol. 49, 3813–3821.

Hu, R., Gong, X., Duan, Y., Li, N., Che, Y., Cui, Y., Zhou, M., Liu, C., Wang, H., Hong, F., 2010. Neurotoxicological effects and the impairment of spatial recognition memory in mice caused by exposure to TiO_2 nanoparticles. Biomaterials 31, 8043–8050.

Lee, J.H., Kim, Y.S., Song, K.S., Ryu, H.R., Sung, J.H., Park, J.D., Park, H.M., Song, N.W., Shin, B.S., Marshak, D., Ahn, K., Lee, J.E., Yu, I.J., 2013. Biopersistence of silver nanoparticles in tissues from Sprague-Dawley rats. Part. Fibre Toxicol 10.

Li, G., Simon, M.J., Cancel, L.M., Shi, Z.D., Ji, X., Tarbell, J.M., Morrison 3rd, B., Fu, B.M., 2010. Permeability of endothelial and astrocyte cocultures: in vitro blood-brain barrier models for drug delivery studies. Ann. Biomed. Eng. 38, 2499–2511.

Lin, Z., Monteiro-Riviere, N.A., Riviere, J.E., 2015. Pharmacokinetics of metallic nanoparticles. Wiley Interdiscip. Rev. Nanomed. Nanobiotechnol. 7, 189–217.

Liu, Y., Xu, Z., Li, X., 2013. Cytotoxicity of titanium dioxide nanoparticles in rat neuroglia cells. Brain Inj. 27, 934–939.

Liu, D., Lin, B., Shao, W., Zhu, Z., Ji, T., Yang, C., 2014. In vitro and in vivo studies on the transport of PEGylated silica nanoparticles across the blood-brain barrier. ACS Appl. Mater. Interfaces 6, 2131–2136.

Loeschner, K., Hadrup, N., Qvortrup, K., Larsen, A., Gao, X., Vogel, U., Mortensen, A., Lam, H.R., Larsen, E.H., 2011. Distribution of silver in rats following 28 days of repeated oral exposure to silver nanoparticles or silver acetate. Part. Fibre Toxicol. 8, 18.

Maynard, A.D., 2014. A decade of uncertainty. Nat. Nanotechnol. 9, 159–160.

Mohammadipour, A., Fazel, A., Haghir, H., Motejaded, F., Rafatpanah, H., Zabihi, H., Hosseini, M., Bideskan, A.E., 2014. Maternal exposure to titanium dioxide nanoparticles during pregnancy; impaired memory and decreased hippocampal cell proliferation in rat offspring. Environ. Toxicol. Pharmacol. 37, 617–625.

Montiel-Davalos, A., Ventura-Gallegos, J.L., Alfaro-Moreno, E., Soria-Castro, E., Garcia-Latorre, E., Cabanas-Moreno, J.G., del Pilar Ramos-Godinez, M., Lopez-Marure, R., 2012. TiO(2) nanoparticles induce dysfunction and activation of human endothelial cells. Chem. Res. Toxicol. 25, 920–930.

Murdock, R.C., Braydich-Stolle, L., Schrand, A.M., Schlager, J.J., Hussain, S.M., 2008. Characterization of nanomaterial dispersion in solution prior to in vitro exposure using dynamic light scattering technique. Toxicol. Sci. 101, 239–253.

Naik, P., Cucullo, L., 2012. In vitro blood-brain barrier models: current and perspective technologies. J. Pharm. Sci. 101, 1337–1354.

Nitta, T., Hata, M., Gotoh, S., Seo, Y., Sasaki, H., Hashimoto, N., Furuse, M., Tsukita, S., 2003. Size-selective loosening of the blood-brain barrier in claudin-5-deficient mice. J. Cell Biol. 161, 653–660.

Obermeier, B., Daneman, R., Ransohoff, R.M., 2013. Development, maintenance and disruption of the blood-brain barrier. Nat. Med. 19, 1584–1596.

Onodera, A., Nishiumi, F., Kakiguchi, K., Tanaka, A., Tanabe, N., Honma, A., Yayama, K., Yoshioka, Y., Nakahira, K., Yonemura, S., Yanagihara, I., Tsutsumi, Y., Kawai, Y., 2015. Short-term changes in intracellular ROS localisation after the silver nanoparticles exposure depending on particle size. Toxicol. Rep. 2, 574–579.

Park, E.J., Bae, E., Yi, J., Kim, Y., Choi, K., Lee, S.H., Yoon, J., Lee, B.C., Park, K., 2010. Repeated-dose toxicity and inflammatory responses in mice by oral administration of silver nanoparticles. Environ. Toxicol. Pharmacol. 30, 162–168.

Rai, M., Yadav, A., Gade, A., 2009. Silver nanoparticles as a new generation of antimicrobials. Biotechnol. Adv. 27, 76–83.

Seok, S.M., Kim, J.M., Park, T.Y., Baik, E.J., Lee, S.H., 2013. Fructose-1,6-bisphosphate ameliorates lipopolysaccharide-induced dysfunction of blood-brain barrier. Arch. Pharm. Res. 36, 1149–1159.

Sharma, A., Muresanu, D.F., Patnaik, R., Sharma, H.S., 2013. Size- and age-dependent neurotoxicity of engineered metal nanoparticles in rats. Mol. Neurobiol. 48, 386–396.

Sheng, W.S., Hu, S., Feng, A., Rock, R.B., 2013. Reactive oxygen species from human astrocytes induced functional impairment and oxidative damage. Neurochem. Res. 38, 2148–2159.

Shi, J., Sun, X., Lin, Y., Zou, X., Li, Z., Liao, Y., Du, M., Zhang, H., 2014. Endothelial cell injury and dysfunction induced by silver nanoparticles through oxidative stress via IKK/NF-kappaB pathways. Biomaterials 35, 6657–6666.

Shin, K., Fogg, V.C., Margolis, B., 2006. Tight junctions and cell polarity. Annu. Rev. Cell Dev. Biol. 22, 207–235.

Skalska, J., Frontczak-Baniewicz, M., Struzynska, L., 2015. Synaptic degeneration in rat brain after prolonged oral exposure to silver nanoparticles. Neurotoxicology 46, 145–154.

Song, Y., Li, X., Du, X., 2009. Exposure to nanoparticles is related to pleural effusion, pulmonary fibrosis and granuloma. Eur. Respir. J. 34, 559–567.

Song, J., Kang, S.M., Lee, W.T., Park, K.A., Lee, K.M., Lee, J.E., 2014. Glutathione protects brain endothelial cells from hydrogen peroxide-induced oxidative stress by increasing Nrf2 expression. Exp. Neurobiol. 23, 93–103.

Stamatovic, S.M., Keep, R.F., Kunkel, S.L., Andjelkovic, A.V., 2003. Potential role of MCP-1 in endothelial cell tight junction 'opening': signaling via Rho and Rho kinase. J. Cell Sci. 116, 4615–4628.

Sun, C., Yin, N., Wen, R., Liu, W., Jia, Y., Hu, L., Zhou, Q., Jiang, G., 2016. Silver nanoparticles induced neurotoxicity through oxidative stress in rat cerebral

astrocytes is distinct from the effects of silver ions. Neurotoxicology 52, 210–221.
Suzuki, H., Toyooka, T., Ibuki, Y., 2007. Simple and easy method to evaluate uptake potential of nanoparticles in mammalian cells using a flow cytometric light scatter analysis. Environ. Sci. Technol. 41, 3018–3024.
Takenaka, S., Karg, E., Roth, C., Schulz, H., Ziesenis, A., Heinzmann, U., Schramel, P., Heyder, J., 2001. Pulmonary and systemic distribution of inhaled ultrafine silver particles in rats. Environ. Health Perspect. 109, 547–551.
Tang, J.L., Xiong, L., Wang, S., Wang, J.Y., Liu, L., Li, J.G., Yuan, F.Q., Xi, T.F., 2009. Distribution, translocation and accumulation of silver nanoparticles in rats. J. Nanosci. Nanotechnol. 9, 4924–4932.
Trickler, W.J., Lantz, S.M., Murdock, R.C., Schrand, A.M., Robinson, B.L., Newport, G.D., Schlager, J.J., Oldenburg, S.J., Paule, M.G., Slikker Jr., W., Hussain, S.M., Ali, S.F., 2010. Silver nanoparticle induced blood-brain barrier inflammation and increased permeability in primary rat brain microvessel endothelial cells. Toxicol. Sci. 118, 160–170.
Van Itallie, C., Rahner, C., Anderson, J.M., 2001. Regulated expression of claudin-4 decreases paracellular conductance through a selective decrease in sodium permeability. J. Clin. Invest. 107, 1319–1327.
Wang, J.X., Liu, Y., Jiao, F., Lao, F., Li, W., Gu, Y.Q., Li, Y.F., Ge, C.C., Zhou, G.Q., Li, B., Zhao, Y.L., Chai, Z.F., Chen, C.Y., 2008. Time-dependent translocation and potential impairment on central nervous system by intranasally instilled TiO_2 nanoparticles. Toxicology 254, 82–90.
Wilhelm, I., Krizbai, I.A., 2014. In vitro models of the blood-brain barrier for the study of drug delivery to the brain. Mol. Pharm. 11, 1949–1963.
Wu, C.Y., Tu, K.J., Lo, Y.S., Pang, Y.L., Wu, C.H., 2016. Alkaline hydrogen peroxide treatment for TiO_2 nanoparticles with superior water-dispersibility and visible-light photocatalytic activity. Mater. Chem. Phys. 181, 82–89.
Ye, D., Dawson, K.A., Lynch, I., 2015. A TEM protocol for quality assurance of in vitro cellular barrier models and its application to the assessment of nanoparticle transport mechanisms across barriers. Analyst 140, 83–97.
Yuan, S.Y., R.R, 2010. Regulation of Endothelial Barrier Function. Morgan & Claypool Life Sciences, San Rafael, CA.
Ze, Y., Hu, R., Wang, X., Sang, X., Ze, X., Li, B., Su, J., Wang, Y., Guan, N., Zhao, X., Gui, S., Zhu, L., Cheng, Z., Cheng, J., Sheng, L., Sun, Q., Wang, L., Hong, F., 2014a. Neurotoxicity and gene-expressed profile in brain-injured mice caused by exposure to titanium dioxide nanoparticles. J. Biomed. Mater. Res. A 102, 470–478.
Ze, Y.G., Sheng, L., Zhao, X.Y., Hong, J., Ze, X., Yu, X.H., Pan, X.Y., Lin, A., Zhao, Y., Zhang, C., Zhou, Q.P., Wang, L., Hong, F.S., 2014b. TiO2 nanoparticles induced hippocampal neuroinflammation in mice. PLoS One 9.
Zehendner, C.M., Librizzi, L., Hedrich, J., Bauer, N.M., Angamo, E.A., de Curtis, M., Luhmann, H.J., 2013. Moderate hypoxia followed by reoxygenation results in blood-brain barrier breakdown via oxidative stress-dependent tight-junction protein disruption. PLoS One 8, e82823.
van der Zande, M., Vandebriel, R.J., Van Doren, E., Kramer, E., Herrera Rivera, Z., Serrano-Rojero, C.S., Gremmer, E.R., Mast, J., Peters, R.J., Hollman, P.C., Hendriksen, P.J., Marvin, H.J., Peijnenburg, A.A., Bouwmeester, H., 2012. Distribution, elimination, and toxicity of silver nanoparticles and silver ions in rats after 28-day oral exposure. ACS Nano 6, 7427–7442.